Applied Catalysis B: Environmental 304 (2022) 120999

Contents lists available at ScienceDirect

Applied Catalysis B: Environmental

journal homepage: www.elsevier.com/locate/apcatb

Unique functionalities of carbon shells coating on $ZnFe_2O_4$ for enhanced photocatalytic hydroxylation of benzene to phenol

Baoying Yang , Shikun Zhang , Yan Gao , Lianqi Huang , Can Yang , Yidong Hou *, Jinshui Zhang *

State Key Laboratory of Photocatalysis on Energy and Environment, College of Chemistry, Fuzhou University, 2 Xueyuan Road, University Town, Fuzhou 350108, China

ARTICLE INFO

Keywords:
Carbon-encapsulated $ZnFe_2O_4$
Photocatalysis
Phenol production
Hydroxylation reaction
Charge separation
Photo-fenton

ABSTRACT

Hydroxylation of benzene to phenol over a photocatalyst is a green approach toward phenol production. $ZnFe_2O_4$ (ZFO) with an intrinsic peroxidase-like catalytic behavior toward H_2O_2 activation is an emerging photocatalyst for benzene hydroxylation reaction; however, its catalytic performance is greatly limited by the fast charge recombination, inevitable metal leaching and hydrophilic surface structure. Herein, the encapsulation of ZFO by carbons (ZFO@C) is an effective solution to address these issues. The carbons conformably coating on ZFO not only protect them from corrosion and metal leaching, but also enable the generation of a strong electronic contact between them to facilitate charge separation. In addition, the carbons also increase the surface affinity for benzene adsorption. As a result, ZFO@C exhibited a significant enhanced photocatalytic activity and durability for phenol synthesis. Furthermore, ZFO@C with carbon derived unique functionalities will have a broad application in photocatalytic green synthesis of fine chemicals.

1. Introduction

Phenol is a raw chemical feedstock widely used in the production of drugs, dyes, and functional polymers [1–5]. Currently, phenol is mainly synthesized from cumene via a multi-step process, which suffers from several issues including a low yield of phenol (~ 5%), large energy consumption and severe equipment corrosion [6–10]. Recently, the direct hydroxylation of benzene to phenol over visible-light responsive photocatalysts using H_2O_2 as the oxidant has attracted much attention, due to the high atomic utilization and the ability to utilize clean and safe solar energy [11–14]. Generally, the photocatalytic hydroxylation of benzene to phenol is closely relied on the generation of massive ·OH from H_2O_2 decomposition in a Fenton manner over a photocatalyst [15–17]. The generated ·OH then attacks the aromatic ring to produce phenol [15,18–20]. The development of photocatalysts with an excellent catalytic ability toward H_2O_2 activation therefore is of essential for the photocatalytic benzene hydroxylation reaction.

Spinel $ZnFe_2O_4$ (ZFO) has been widely applied in the fields of solar energy utilization, such as hydrogen production and organic pollutant photodegradation [21,22], because of its excellent properties including low toxicity, abundance, and visible-light responsive [23–26]. Recently, ZFO has been employed for photo-Fenton activation of H_2O_2, owing to its intrinsic peroxidase-like catalytic behavior [21,25,27,28]. To this end, ZFO would be a promising candidate for photocatalytic phenol synthesis. However, its photocatalytic performance for phenol synthesis is limited by inherent properties of ZFO. For example, the hydrophilic surface with abundant bonded-OH groups disfavors for the adsorption of nonpolar benzene and the desorption of polar phenol, thus resulting in a low yield with a poor selectivity toward phenol synthesis [18,29,30]; the inevitable leaching of metal species leads to the decomposition and fast deactivation of ZFO during heterogeneous Fenton process [31–33]. In addition, the high recombination rates of photoinduced charges result in a low activity of phenol yield, thus leading to a poor efficiency of solar energy conversion [34–37]. Hence, the well addressing of the above issues is of great crucial to advance ZFO for photocatalytic benzene hydroxylation to produce phenol.

Herein, the construction of ultrathin carbon layers onto ZFO (ZFO@C) is demonstrated as a simple yet effective strategy to solve the inherent issues encountered in the application of ZFO for photocatalytic benzene hydroxylation reaction, due to the unique structural functionalities derived from ultrathin carbon layers [38–41]. In Scheme 1, the hydrophobic carbons with π-conjugated electron system favor for benzene selective adsorption other than phenol to facilitate the kinetic control of hydroxylation reaction [42–44]. This is of beneficial to enhance the phenol yield with improved selectivity. These conformably coated carbon layers with excellent structural rigidity can also function

* Corresponding authors.
E-mail addresses: ydhou@fzu.edu.cn (Y. Hou), jinshui.zhang@fzu.edu.cn (J. Zhang).

https://doi.org/10.1016/j.apcatb.2021.120999
Received 14 October 2021; Received in revised form 29 November 2021; Accepted 5 December 2021
Available online 7 December 2021

as a robust protective shell to prevent ZFO from corrosion and aggregation, thus well addressing the issue of metal leaching to afford a long-term operation of ZFO@C in photocatalytic hydroxylation process [45–47]. In addition, the carbon layers intimate adhering on ZFO surface can quickly accept electrons from the conductor band of ZFO, thus greatly promoting electron-hole pairs separation to minimize the energy-wasteful charge recombination [38,48,49]. As a result of these unique functionalities of ultrathin carbon shells, ZFO@C exhibited a significant enhanced photocatalytic activity and durability for phenol synthesis. Furthermore, ZFO@C with carbon derived unique functionalities will have a broad application in photocatalytic green synthesis of fine chemicals.

2. Materials and methods

2.1. Synthesis of ZFO

Typically, a 60 mL solution containing $Zn(NO_3)_2$ (2.5 mmol) and $Fe(NO_3)_3$ (5 mmol) was prepared and adjusted to a pH value of 9 using NaOH solution. After being stirred for 1 h, it was treated in an autoclave at 180 °C for 10 h. The obtained suspension was washed and dried at 60 °C overnight. The as-prepared sample was labeled as ZFO.

2.2. Synthesis of ZFO@C

Typically, a 60 mL solution containing $Zn(NO_3)_2$ (2.5 mmol) and $Fe(NO_3)_3$ (5 mmol) was prepared, followed by adding with a certain amount of glucose. The mixture was adjusted to a pH value of 9 using NaOH solution. After being stirred for 1 h, it was treated in an autoclave at 180 °C for 10 h. The obtained suspension was washed and dried at 60 °C overnight. These products were labeled as ZFO@C-x, where x = 1, 2 and 3 refereed to the mass of glucose such as 50, 100 and 200 mg used in the synthesis.

2.3. Characterization

Bruker D8 Advance diffractometer, LabRAM HR Evolution Raman spectrometer, Perkin-Elmer 4500 fluorescence spectrophotometer and Nicolet Is50 spectrometer were employed for the collection of X-ray diffraction (XRD) patterns, Raman spectra, photoluminescence (PL) spectra and Fourier Transform infrared spectroscopy (FTIR) spectra, respectively. The optical properties were studied by Cary 5000 in a range of 300–800 nm. The scanning electron microscopies (SEM) equipment is JSM-6700F. The transmission electron microscopy (TEM) equipment is FEI Talos F200S X-ray photoelectron spectroscopy (XPS) is Thermo ESCALAB250. Bruker model A300 spectrometer was employed for Electron paramagnetic resonance (EPR) study.

2.4. Photocatalytic activity examination

Typically, 30 mg catalyst was added to a condenser-equipped flask reactor containing 3 mL water, 3 mL acetonitrile, 0.5 mL hydrogen peroxide (30 wt%) and 0.1 mL benzene. The reaction mixture was irradiated by a 300 W Xe lamp (420 nm cutoff filter) with stirring. The reaction was quenched by ethanol (3 mL). The products were analyzed by HPLC (Agilent 1260).

3. Results and discussion

3.1. Characterization of ZFO@C

The XRD patterns of ZFO and ZFO@C are displayed in Fig. 1a. The peaks at 2θ = 29.9, 35.3, 42.8, 53.2, 56.6, 62.2 and 73.5° were assigned to the characteristic diffractions of spinel $ZnFe_2O_4$ [50,51], indicating the successful formation of $ZnFe_2O_4$, even in the starting solutions containing glucose as carbon precursor. This stated that the process of carbon shell construction cannot influence the evolution of spinel phase $ZnFe_2O_4$, which was very important for the construction of ZFO@C for photocatalytic hydroxylation reaction. An evident broadened of the diffraction peaks was observed, indicating the grain size of ZFO@C was very small, which was further confirmed by the observation of SEM and TEM images (Figs. 2 and 3). Their average grain size was determined about 12 nm based on (311) diffraction peak by Scherrer equation ($D = 0.9\lambda/\beta\cos\theta$) [36,52]. There were no diffraction peaks ascribed to carbons observed for ZFO@C, but the intensity of ZFO diffractions decreased gradually as increasing the amount of glucose in the starting materials, presumably due to the formation of carbon layers coating on ZFO [40].

In Fig. 1b, Raman spectra were collected to further confirm the present of carbon shells on ZFO. The featured bands assigned to the D and G band of carbons were observed for ZFO@C, while were absent for pristine ZFO [53–55]. This observation clearly suggested the present of carbon in ZFO@C. In Fig. 1c, the formation of carbon shells on ZFO was also demonstrated by FTIR spectra. For pristine ZFO, the absorption at 1640 cm^{-1} was attribute to O-H. For ZFO@C, this peak became less intensity, accompanied with two new peaks such as 1390 and 1610 cm^{-1}. They were ascribed to the vibration of C-C and/or C═C bonds [56,57]. The intensity of these two new peaks increased as increasing the amount

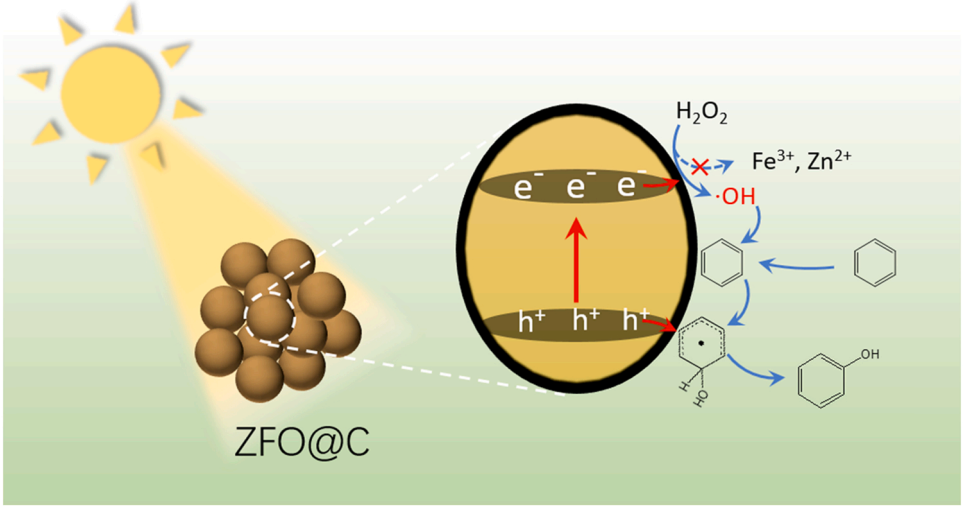

Scheme 1. Photocatalytic hydroxylation of benzene to phenol over ZFO@C.

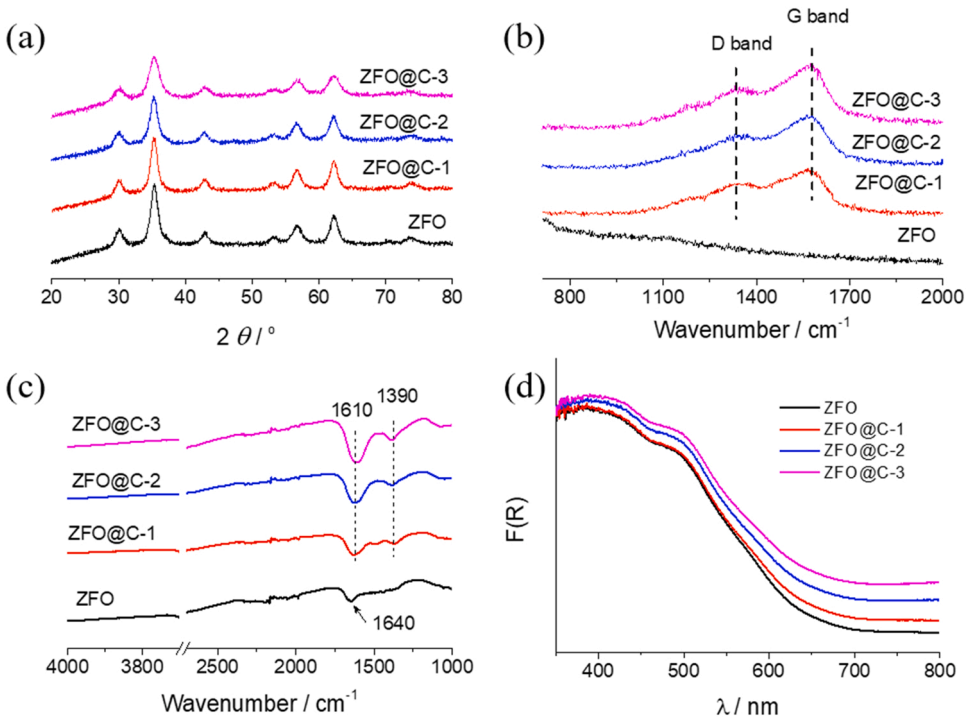

Fig. 1. (a) XRD patterns, (b) Raman spectra, (c) FTIR spectra and (d) UV-Vis diffuse reflectance spectra of ZFO and ZFO@C.

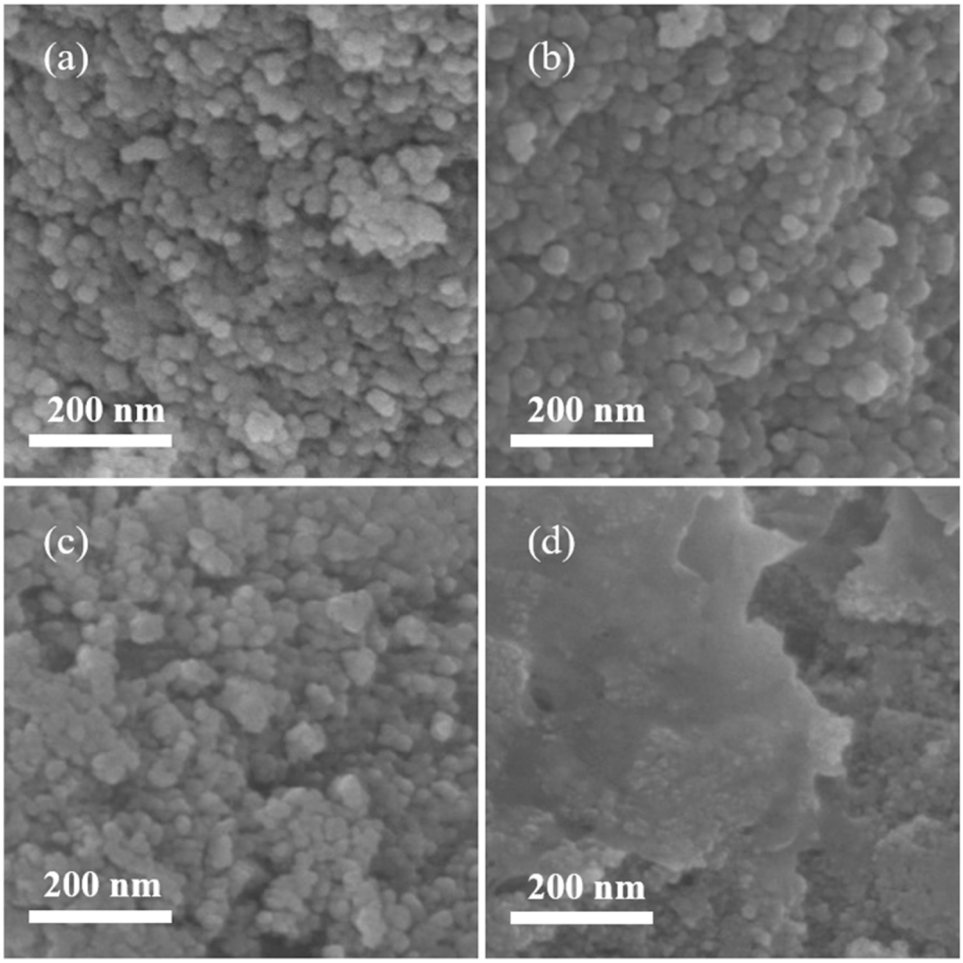

Fig. 2. SEM images obtained from (a) ZFO, (b) ZFO@C-1, (c) ZFO@C-2 and. (d) ZFO@C-3.

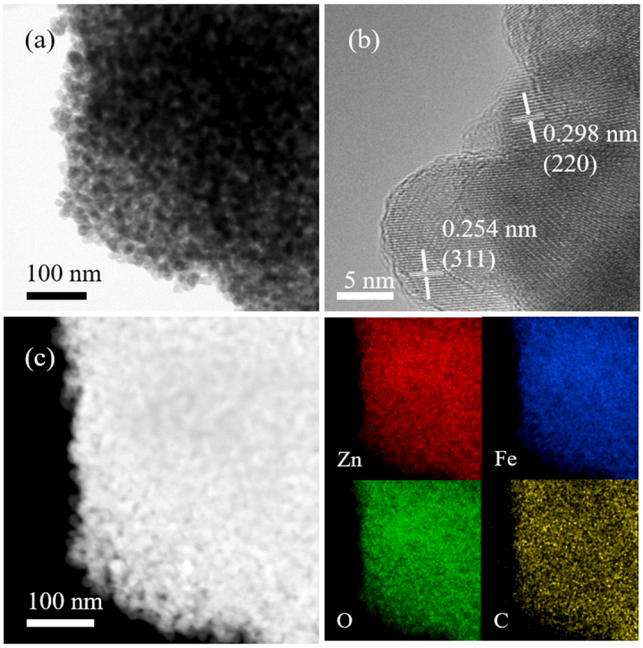

Fig. 3. (a) TEM, (b) HR-TEM and (c) element mapping images of ZFO@C-2.

of glucose in starting materials to generate carbon shells.

The influence of assembly carbon shells on optical properties of ZFO was studied by UV-Vis DRS. In Fig. 1d, ZFO@C exhibited a typical semiconductor absorption, indicating the well development of semiconductor band structure in ZFO@C even in the present of glucose in the starting materials. Comparison with pristine ZFO, the absorption edge of ZFO@C red-shifted gradually as increasing the amount of glucose in the starting materials, due to the surface hybridization of ZFO with carbon shells [21,40]. The bandgap energy of ZFO@C-1, −2, −3 was calculated to be 1.87, 1.82 and 1.78 eV (Fig. S1), respectively, which were smaller than that of 1.90 eV for ZFO. Evidently, the carbon shells coating on ZFO also exhibited an absorption from 650 to 800 nm, due to the strong light harvesting behavior of carbon materials. This enhanced light absorption should not be beneficial for photocatalysis.

3.2. Morphology and nanostructure of ZFO@C

Fig. 2 displays the SEM images of ZFO and ZFO@C. In Fig. 2a, ZFO was composed by nanoparticles with size of ~15 nm, in consist with calculation from XRD patterns. For ZFO@C series (Fig. 2b–d), their morphologies were closely depended on the concentration of glucose in the starting solution. For example, individual nanoparticles were observed for ZFO@C-1, similar to the observation of ZFO. For ZFO@C-2, partially combined nanoparticles were observed. For ZFO@C-3, significantly combined nanoparticles were observed, since too much glucose left in the solution would cause glucose/carbon accumulation. This observation also demonstrated that the glucose molecules in low concentration prefer to assembly carbon layers on ZFO, rather than the formation of carbon agglomerates. Hence, the hydrothermal treatment of glucose containing solution is a unique synthetic strategy to construcure carbon layers on solid particles.

In Fig. 3, TEM images were also conducted to study the nanostructure of ZFO@C. Similar to the observation from SEM images (Fig. 2), ~ 15 nm nanoparticles were observed for ZFO@C-2 (Fig. 3a), as same as that of pristine ZFO (Fig. S2a). Different from the observation of pristine ZFO where no coating layers exhibited on ZFO surface (Fig. S3a), ultrathin carbon layers conformably coating on ZFO surface were clearly identified for ZFO@C (Fig. S3b) [58], which would facilitate to generate the intimate electronic contact between ZFO and carbon shells to promote charge separation. In the high-resolution TEM image (Fig. 3b), lattice fringes such as the ones with 0.298 and 0.254 nm interplanar spacing were assigned to the (220) and (311) planes of spinel ZFO, indicating the evolution of well-developed crystal structure in ZFO@C. This finding is in good consist with the results of XRD patterns. The element mapping images confirmed the homogeneous distribution of Zn, Fe, O and C elementals in ZFO@C (Fig. 3c).

3.3. XPS analysis

Fig. 4 is the XPS spectra obtained from ZFO and ZFO@C. For Zn 2p spectra (Fig. 4a), the peaks with binding energies at 1021.2 and 1044.2 eV were attributed to the characteristic peaks of Zn $2p_{3/2}$ and Zn $2p_{1/2}$ for Zn^{2+}, respectively [21,59]. For Fe 2p spectra (Fig. 4b), the peaks were deconvoluted into the ones assigned to Fe^{2+} or Fe^{3+} species. For example, the ones with binding energies at 713.1 and 727.2 eV were assigned to Fe $2p_{3/2}$ and Fe $2p_{1/2}$ of Fe^{3+} species; the ones with binding energies at 710.3 and 724.4 eV were for the Fe $2p_{3/2}$ and Fe $2p_{1/2}$ of Fe^{2+} species [60–63]; the other four peaks were the satellite peaks. For O 1s spectra (Fig. 4c), the peaks at 529.7, 531.6, and 533.3 eV were attributed to the lattice oxygen, the oxygen species containing in O-H and C–O/C═O bonds, respectively [21]. For C 1s spectra (Fig. 4d), the peaks at 284.6, 286.2, and 288.7 eV were belonged to the graphitic carbon, C–O bonds, and C═C/(C═O) bonds [36]. Evidently, the carbon layers coating on ZFO surface exhibited a significant change in these XPS spectra. For example, the intensity of Zn 2p and Fe 2p spectra decreased obviously, since the surface was completely blocked by the conformably coated carbon shells; in comparison with the pristine ZFO, the peaks of Zn 2p and Fe 2p shifted positively, presumably due to the fast transfer of electrons from ZFO to carbon shells. This finding clearly demonstrated the formation of strong electronic contact between ZFO and carbon shells. In O 1s spectra, the signal originating from the lattice oxygen decrease evidently, while the other two in particular the one in C–O/C═O bonds were enhanced greatly. In C 1s spectra, the signal attributed to the graphitic carbon became significantly, again demonstrating the formation of carbon layers on ZFO.

3.4. Structural functionalities of carbon shells

The surface affinity of ZFO with or without carbon shells covering on its surface was studied by the optical contact angle measurements. In Figs. 5a and S4, the water contact angle was determined to be 23.6°, 38.2° and 49.1° for ZFO@C-1, -2 and -3, respectively, closely depended on the thickness of carbon shells coating on ZFO. As comparison, the value obtained from bare ZFO was determined to be 12.9°. This finding indicated that the carbon shells coating on ZFO indeed increase the surface hydrophobicity of ZFO. This would be useful for benzene adsorption [64]. To demonstrated this, contact angles using benzene to replace water were tested. In Figs. 5a and S4, the benzene contact angle decreased from 36.8° for bare ZFO to 22.3, 16.1 and 14.9° for ZFO@C-1, -2, and -3, respectively, clearly stating the better adsorption of benzene on ZFO@C. This was mainly due to the unique functionalities of carbon shells, in particular the hydrophobic surface and π-conjugated electron system [19,64]. In Figs. 5b and S5, the benzene adsorption behavior was further studied by the apparent adsorption of benzene on ZFO and ZFO@C. The benzene adsorption amount was determined to be 1.9, 3, and 3.3 mmol g^{-1} for ZFO@C-1, -2, and -3 respectively, much bigger than that obtained for ZFO (1 mmol g^{-1}). Previous studies proved that the benzene adsorption behavior played a critical role in selectivity hydroxylation of benzene to phenol in liquid-phase. The increase of surface affinity to benzene derived from carbon shells would be beneficial for benzene hydroxylation reaction over ZFO@C photocatalyst [19].

It has been demonstrated that the rigid carbon shells could provide a sufficient protection for metal cores.[19,38] To Figure out whether the ultrathin carbon layers work for protecting ZFO nanoparticles from

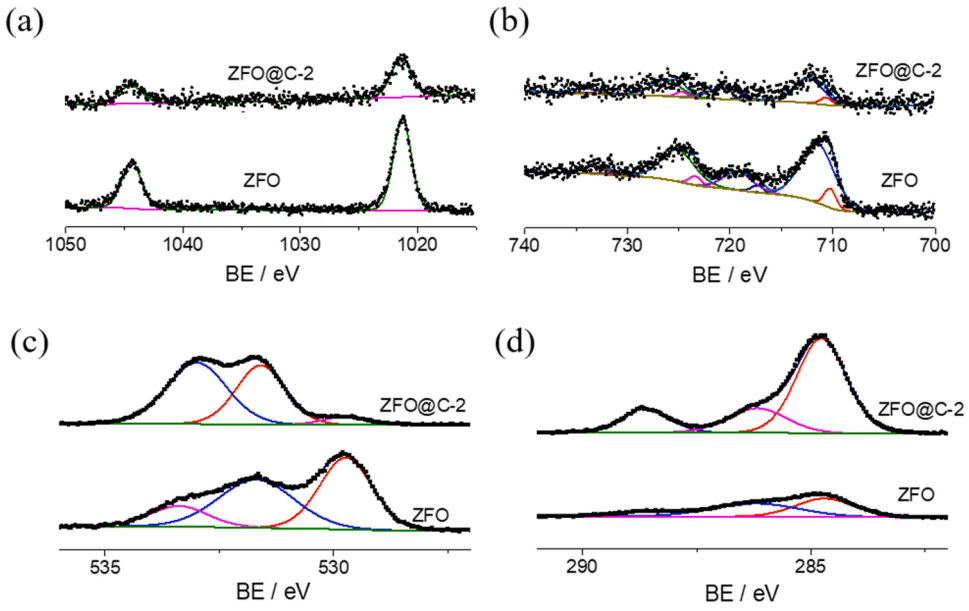

Fig. 4. (a) Zn 2p, (b) Fe 2p, (c) O 1s and (d) C 1s spectra for ZFO and ZFO@C-2.

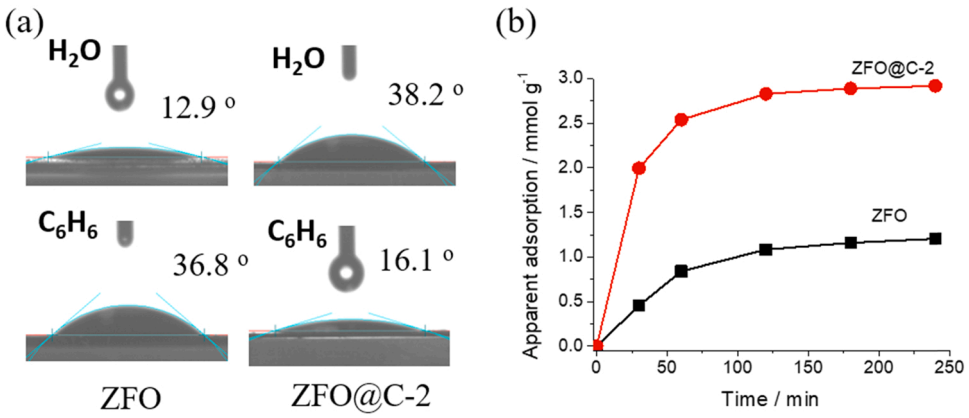

Fig. 5. (a) Optical contact angle measurements obtained on ZFO and ZFO@C-2. (b) Apparent adsorption behavior of ZFO and ZFO@C-2 toward benzene.

leaching, an acid etching treatment in 1 M HCl for 4 h was carried out. For bare ZFO, the solids particles were almost dissolved with the color changing to orange; while for ZFO@C, the solids particles were well maintained, and no color change of the acid solution was observed (Fig. 6a). This observation was further confirmed by the ICP measurements of the acid solutions (Fig. 6b), in which the concentration of Zn and Fe irons obtained on ZFO was rather higher than that of ZFO@C, clearly speaking that the carbon layers conformably coating on ZFO nanoparticles could well protect them from metal leaching. In Fig. 6c and d, the XRD patterns of ZFO and ZFO@C before and after HCl etching again proved the excellent protective effect of carbon layer for ZFO photocatalysts. For heterogenous benzene hydroxylation reaction, this enhanced stability was highly desirable, which enabled the long-term operation of ZFO@C for photocatalytic phenol synthesis.

The charge separation behavior of ZFO and ZFO@C was investigated by PL spectra [65,66]. In Figs. 7a and S6, the otherwise strong PL emission centering at 400 nm is observed for ZFO, indicating a serious recombination of photoexcited electron-holes happening in ZFO [50]. After being surface coated with carbon layers, the PL spectra quenches quickly, clearly demonstrating that the suppression of charge recombination by electrons transferring from ZFO to carbon shells [38]. This enhanced charge separation in ZFO@C was further proved by the generation of photocurrent. In Figs. 7b and S7, ZFO@C generated a bigger anodic photocurrent over ZFO, indicating that an improved charge separation at semiconductor/water interfaces had been achieved after being surface coated with carbon layers. For heterogenous photocatalysis occurring in liquid phase such as directly benzene hydroxylation reaction, this improved charge separation is rather beneficial to enhance the photocatalytic performance.

3.5. *Photo-fenton activation of H_2O_2*

The activation of H_2O_2 toward ·OH generation to initiate benzene hydroxylation reaction played a predominant role for phenol synthesis in the H_2O_2 involving system [8,15]. In Fig. 8a, EPR measurements using DMPO trapping agent to react with ·OH free radicals were conducted [15]. In dark, rather poor signals were generated; while under light irradiation, a typical spectrum of DMPO-·OH adduct was observed, indicating that·OH was successfully generated by ZFO and ZFO@C catalyzed H_2O_2 decomposition. This clearly spoken the intrinsic peroxidase-like behavior toward H_2O_2 activation under light irradiation. In Fig. S8, the signals of DMPO-·OH adduct had been enhanced, owing to the improved charge separation by intimate coated carbon layers. This improved photo-Fenton behavior of ZFO@C toward H_2O_2 activation was further confirmed by PL spectra using terephthalic acid (TA) to react with·OH (TAOH) [64]. In Fig. 8b, the PL intensity of TAOH obtained on

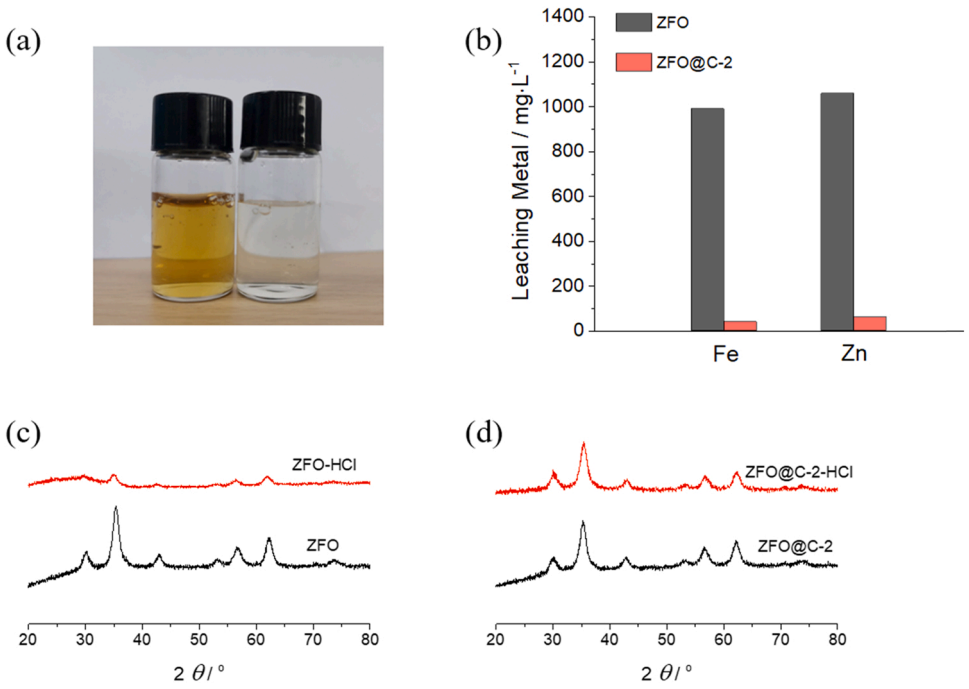

Fig. 6. (a) Photograph of ZFO (left) and ZFO@C-2 (right) after being acid etched in 1 M HCl for 4 h; (b) ICP results of Fe and Zn leaching from ZFO and ZFO@C-2 during acid etching; (c) XRD patterns of ZFO before and after acid etching; (d) XRD patterns of ZFO@C-2 before and after acid etching treatment.

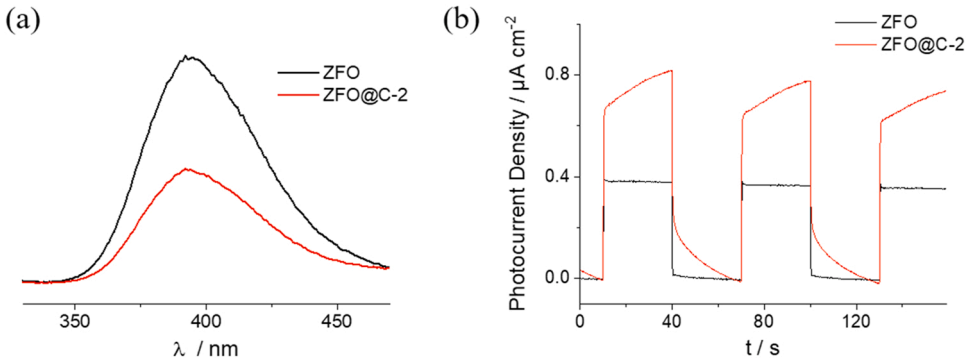

Fig. 7. (a) PL spectra and (b) Photocurrent generation of ZFO and ZFO@C-2.

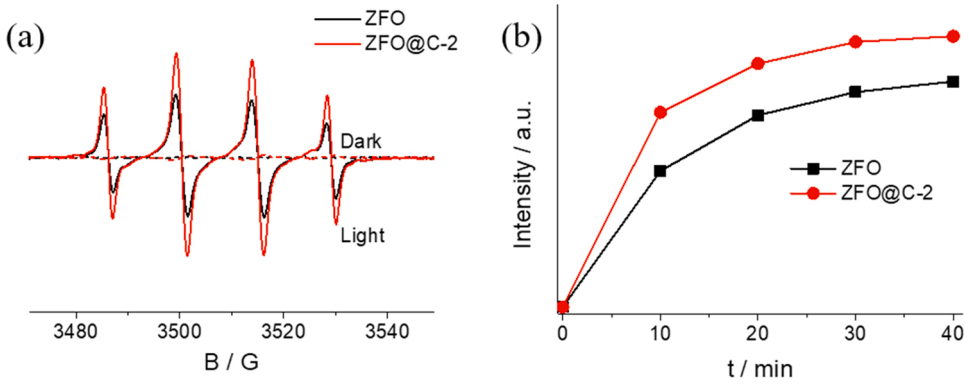

Fig. 8. (a) DMPO spin-trapping EPR spectra, (b) PL spectra of ·OH radical generation of ZFO and ZFO@C-2.

ZFO@C was much higher than that of ZFO, indicating that much more·OH radicals had been generated. This improved catalytic ability toward·OH generation from H_2O_2 decomposition over ZFO@C would be favorable for photocatalytic hydroxylation of benzene [19]. It should be pointed out that too much carbon layers coating on ZFO would inhibit the activation of H_2O_2, see ZFO@C-3 in Fig. S8. This would counteract the promote effect of carbon functionalities such as enhanced benzene adsorption for benzene hydroxylation reaction.

3.6. Photocatalytic benzene hydroxylation performance

In Table 1, the unique functionalities of carbon shells for photocatalytic phenol synthesis were evaluated by reactions proceeding in water/acetonitrile biphasic system using H_2O_2 oxidant. In dark, the phenol yield obtained on ZFO (Entry 1) and ZFO@C (Entry 3) was rather low (~ 0.3%); without H_2O_2, only a trace amount of phenol was produced (< 0.1%, Entry 5); when both of visible-light irradiation and H_2O_2 were involved, the yield increased significantly (> 8.0%, Entry 2, 4, 6 and 7), exhibiting a typical photo-Fenton catalytic behavior toward phenol synthesis [21]. This finding was in consist with the results of EPR measurements where little·OH radicals were generated in dark to drive hydroxylation reactions (Fig. 8a). In Entry 8 and 9, the hydroxylation reactions happened in acetonitrile or water single phasic system were carried out. As compared to the reaction proceeding in the biphasic system, the photocatalytic performance, in particular the selectivity decreased evidently, underling the advantages of water/acetonitrile biphasic system for liquid-phase benzene hydroxylation reaction [64]. In Fig. 9, an obvious deactivation in photocatalytic performance was discovered for pristine ZFO, where the phenol yield decreased from 8.6% in 1st run to 4.7% in 5th run with a selectivity of 76.3%. This activity loss was mainly due to the catalyst corrosion and the metal leaching from ZFO. For ZFO@C series, a typical activation of ZFO@C in 1st run was involved, which was similar to the observation from other core-shells nanostructured catalysts such as Fe@C and $FeVO_4$ @OS for benzene hydroxylation reactions [19,64]. Evidently, their photocatalytic performance was closely depended on the thickness of carbon shells coating on the surface. For ZFO@C-1, the content of carbons was not enough to achieve the complete encapsulation of ZFO nanoparticles, thus still encountering the issue of metal leaching to gradually deactivate the photocatalysts. For ZFO@C-2, as a result of conformably encapsulated by ultrathin carbon layers, it exhibited a significant promotion effect derived from the structural functionalities of carbon shells for photocatalytic phenol synthesis [19,21,38]. For example, the improved charge separation and enhanced benzene adsorption leaded to a yield of 15.8% for phenol production with a selectivity of 99.4%, which was much better than that of pristine ZFO. In addition, the effective suppression of metal leaching afforded a robust stability for benzene hydroxylation reaction in a five-run catalytic performance (Figs. S9–12). For ZFO@C-3, although it still maintained a good stability in multiple runs of hydroxylation reactions, the yield of phenol decreased to 12.1%. This decreased performance was mainly due to the inhibition of H_2O_2 activation by too thick carbon layers coating on its surface. Hence, the surface modification of ZFO nanoparticles with conformably coated ultrathin carbon layers to utilize the unique functionalities of carbon shells was a unique strategy to advance ZFO nanophotocatalysts for phenol synthesis.

4. Conclusions

In conclusion, the encapsulation of ZFO nanocrystallines by ultrathin carbon layers is a simply yet effective strategy to utilize the unique functionalities of carbon shells to address the issues encountered in photocatalytic benzene hydroxylation reaction. For example, the ultrathin carbon shells intimate adhering on ZFO surface can generate a strong electronic contact between them promote electron transfer from ZFO to carbon shells, thus minimizing the energy-wasteful charge recombination. In addition, the conformable encapsulation of ZFO by rigid carbon shells can keep ZFO from corrosion and metal leaching, which are beneficial to improve the catalytic stability during photocatalytic benzene hydroxylation process; the carbon shells also favor for benzene adsorption to facilitate the kinetic control of hydroxylation reaction. Benefiting from such unique structural functionalities of carbon shells, ZFO@C exhibited a significant enhanced photocatalytic activity and durability for phenol synthesis. Furthermore, ZFO@C with carbon derived unique functionalities will have a broad application in photocatalytic green synthesis of fine chemicals [67,68].

Table 1
Photocatalytic hydroxylation of benzene to phenol over ZFO and ZFO@C[a].

Entry	Photocatalyst	Light	Phenol Yield / %	Phenol Selectivity / %
1	ZFO	–	0.2	74.9
2[b]	ZFO	+	8.6	79.4
3	ZFO@C-1	–	0.3	79.5
4[b]	ZFO@C-1	+	9.1	90.2
5[c]	ZFO@C-2	+	< 0.1	89.4
6[b]	ZFO@C-2	+	9.4	96.5
7[b]	ZFO@C-3	+	9.3	97.9
8[d]	ZFO@C-2	+	7.4	56.9
9[e]	ZFO@C-2	+	6.5	71.3
10[f]	ZFO	+	6.5	76.5
11[f]	ZFO@C-1	+	10.8	88.4
12[f]	ZFO@C-2	+	15.5	99.4
13[f]	ZFO@C-3	+	11.9	99.5

[a] Reaction conditions: 30 mg photocatalyst, 3 mL water-3 mL acetonitrile, 0.5 mL H_2O_2 (30 wt%,) and 0.1 mL benzene.
[b] 1st run.
[c] Without H_2O_2.
[d] 0 mL water-6 mL acetonitrile.
[e] 6 mL water-0 mL acetonitrile.
[f] 2nd run.

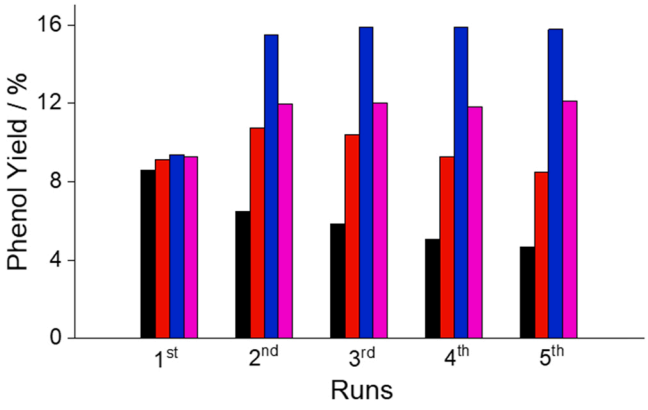

Fig. 9. Photocatalytic synthesis of phenol over ZFO (black), ZFO@C-1 (red), ZFO@C-2 (blue) and ZFO@C-3 (pink) (λ > 420 nm).

CRediT authorship contribution statement

Baoying Yang: Methodology, Investigation, Writing – original draft, Writing – review & editing. **Shikun Zhang:** Investigation, Validation. **Yan Gao:** Data curation, Validation. **Lianqi Huang:** Investigation, Validation. **Can Yang:** Data curation, Writing – review & editing. **Yidong Hou:** Supervision, Writing – review & editing. **Jinshui Zhang:** Conceptualization, Project administration, Supervision, Writing – review & editing.

Declaration of Competing Interest

The authors declare that they have no known competing financial interests or personal relationships that could have appeared to influence the work reported in this paper.

Acknowledgments

We are grateful for the financial support from NSFC (21972022, 22072021 and U1805255), and the 111 Project (D16008).

Appendix A. Supplementary material

XRD patterns, Raman spectra, FTIR spectra, SEM images, TEM image and Elemental mapping images, Zn 2p and Fe 2p XPS spectra, Photocurrent generation, Apparent adsorption behavior, Photoluminescence spectra, EPR spectra and $[F(R)]^2$ versus photo energy spectra.

Appendix B. Supporting information

Supplementary data associated with this article can be found in the online version at doi:10.1016/j.apcatb.2021.120999.

References

[1] S.-i Niwa, M. Eswaramoorthy, J. Nair, A. Raj, N. Itoh, H. Shoji, T. Namba, F. Mizukami, A. One-step, conversion of benzene to phenol with a palladium membrane, Science 295 (2002) 105–107.

[2] Y. Pan, Y. Chen, K. Wu, Z. Chen, S. Liu, X. Cao, W.C. Cheong, T. Meng, J. Luo, L. Zheng, C. Liu, D. Wang, Q. Peng, J. Li, C. Chen, Regulating the coordination structure of single-atom Fe-NxCy catalytic sites for benzene oxidation, Nat. Commun. 10 (2019) 4290.

[3] R. Bal, M. Tada, T. Sasaki, Y. Iwasawa, Direct phenol synthesis by selective oxidation of benzene with molecular oxygen on an interstitial-N/Re cluster/zeolite catalyst, Angew. Chem. Int. Ed. Engl. 45 (2006) 448–452.

[4] O. Shoji, T. Kunimatsu, N. Kawakami, Y. Watanabe, Highly selective hydroxylation of benzene to phenol by wild-type cytochrome P450BM3 assisted by decoy molecules, Angew. Chem. Int. Ed. Engl. 52 (2013) 6606–6610.

[5] T. Zhang, D. Zhang, X. Han, T. Dong, X. Guo, C. Song, R. Si, W. Liu, Y. Liu, Z. Zhao, Preassembly strategy to fabricate porous hollow carbonitride spheres inlaid with single Cu-N_3 sites for selective oxidation of benzene to phenol, J. Am. Chem. Soc. 140 (2018) 16936–16940.

[6] R.J. Schmidt, Industrial catalytic processes—phenol production, Appl. Catal. A: Gen. 280 (2005) 89–103.

[7] G. Ding, W. Wang, T. Jiang, B. Han, H. Fan, G. Yang, Highly selective synthesis of phenol from benzene over a vanadium-doped graphitic carbon nitride catalyst, ChemCatChem 5 (2013) 192–200.

[8] Y. Morimoto, S. Bunno, N. Fujieda, H. Sugimoto, S. Itoh, Direct hydroxylation of benzene to phenol using hydrogen peroxide catalyzed by nickel complexes supported by pyridylalkylamine ligands, J. Am. Chem. Soc. 137 (2015) 5867–5870.

[9] K. Zhang, L. Dai, Y. Liu, J. Deng, L. Jing, K. Zhang, Z. Hou, X. Zhang, J. Wang, Y. Feng, Y. Zhang, H. Dai, Insights into the active sites of chlorine-resistant Pt-based bimetallic catalysts for benzene oxidation, Appl. Catal. B: Environ. 279 (2020), 119372.

[10] Z. Hou, L. Dai, Y. Liu, J. Deng, L. Jing, W. Pei, R. Gao, Y. Feng, H. Dai, Highly efficient and enhanced sulfur resistance supported bimetallic single-atom palladium–cobalt catalysts for benzene oxidation, Appl. Catal. B: Environ. 285 (2021), 119844.

[11] X. Chen, J. Zhang, X. Fu, M. Antonietti, X. Wang, Fe-g-C_3N_4-catalyzed oxidation of benzene to phenol using hydrogen peroxide and visible light, J. Am. Chem. Soc. 131 (2009) 11658–11659.

[12] C. Walling, R.A. Johnson, Fenton's reagent. V. Hydroxylation and side-chain cleavage of aromatics, J. Am. Chem. Soc. 97 (1975) 363–367.

[13] P. Borah, X. Ma, K.T. Nguyen, Y. Zhao, A vanadyl complex grafted to periodic mesoporous organosilica: a green catalyst for selective hydroxylation of benzene to phenol, Angew. Chem. Int. Ed. Engl. 51 (2012) 7756–7761.

[14] L. Balducci, D. Bianchi, R. Bortolo, R. D'Aloisio, M. Ricci, R. Tassinari, R. Ungarelli, Direct oxidation of benzene to phenol with hydrogen peroxide over a modified titanium silicalite, Angew. Chem. Int. Ed. Engl. 42 (2003) 4937–4940.

[15] D. Wang, M. Wang, Z. Li, Fe-based metal–organic frameworks for highly selective photocatalytic benzene hydroxylation to phenol, ACS Catal. 5 (2015) 6852–6857.

[16] Q. Yi, J. Ji, B. Shen, C. Dong, J. Liu, J. Zhang, M. Xing, Singlet oxygen triggered by superoxide radicals in a molybdenum cocatalytic Fenton reaction with enhanced REDOX activity in the environment, Environ. Sci. Technol. 53 (2019) 9725–9733.

[17] C. Dong, J. Ji, B. Shen, M. Xing, J. Zhang, Enhancement of H_2O_2 decomposition by the Co-catalytic effect of WS_2 on the Fenton reaction for the synchronous reduction of Cr(VI) and remediation of phenol, Environ. Sci. Technol. 52 (2018) 11297–11308.

[18] L. Hu, C. Wang, L. Ye, Y. Wu, B. Yue, X. Chen, H. He, Direct hydroxylation of benzene to phenol using H_2O_2 as an oxidant over vanadium-containing mesoporous carbon catalysts, Appl. Catal. A: Gen. 504 (2015) 440–447.

[19] E. Lu, J. Wu, B. Yang, D. Yu, Z. Yu, Y. Hou, J. Zhang, Selective hydroxylation of benzene to phenol over Fe nanoparticles encapsulated within N-doped carbon shells, ACS Appl. Nano Mater. 3 (2020) 9192–9199.

[20] P. Chen, L. Chen, Y. Zeng, F. Ding, X. Jiang, N. Liu, C.-T. Au, S.-F. Yin, Three-dimension hierarchical heterostructure of $CdWO_4$ microrods decorated with Bi_2WO_6 nanoplates for high-selectivity photocatalytic benzene hydroxylation to phenol, Appl. Catal. B: Environ. 234 (2018) 311–317.

[21] F. Wang, Y. Chen, R. Zhu, J. Sun, Novel synthesis of magnetic, porous C/$ZnFe_2O_4$ photocatalyst with enhanced activity under visible light based on the Fenton-like reaction, Dalton Trans. 46 (2017) 11306–11317.

[22] X. Wang, L. Chen, Q. Fan, J. Fan, G. Xu, M. Yan, M.J. Henderson, J. Courtois, K. Xiong, Lactoferrin-assisted synthesis of zinc ferrite nanocrystal: Its magnetic performance and photocatalytic activity, J. Alloy. Compd. 652 (2015) 132–138.

[23] J.M. Won, S.H. Choi, Y.J. Hong, Y.N. Ko, Y.C. Kang, Electrochemical properties of yolk-shell structured $ZnFe_2O_4$ powders prepared by a simple spray drying process as anode material for lithium-ion battery, Sci. Rep. 4 (2014) 5857.

[24] A. Shanmugavani, R.K. Selvan, Synthesis of $ZnFe_2O_4$ nanoparticles and their asymmetric configuration with $Ni(OH)_2$ for a pseudocapacitor, RSC Adv. 4 (2014) 27022.

[25] P. Guo, L. Cui, Y. Wang, M. Lv, B. Wang, X.S. Zhao, Facile synthesis of $ZnFe_2O_4$ nanoparticles with tunable magnetic and sensing properties, Langmuir 29 (2013) 8997–9003.

[26] F. Liu, X. Chu, Y. Dong, W. Zhang, W. Sun, L. Shen, Acetone gas sensors based on graphene-$ZnFe_2O_4$ composite prepared by solvothermal method, Sens. Actuators B: Chem. 188 (2013) 469–474.

[27] L. Su, J. Feng, X. Zhou, C. Ren, H. Li, X. Chen, Colorimetric detection of urine glucose based $ZnFe_2O_4$ magnetic nanoparticles, Anal. Chem. 84 (2012) 5753–5758.

[28] A.S. Saleemi, M. Hafeez, A. Munawar, N. Akhtar, W. Abbas, M.E. Mazhar, Z. Shafiq, A.P. Davis, S.-L. Lee, Synthesis and sensing efficiency of CN-wrapped $ZnFe_2O_4$ microsphere–ionic liquid composites towards ultra-high sensitive arsenic(iii) monitoring of ground drinking water, J. Mater. Chem. C. 8 (2020) 12984–12992.

[29] J. Li, L. Zhang, J. Li, P. An, Y. Hou, J. Zhang, Nanoconfined growth of carbon-encapsulated cobalts as cocatalysts for photocatalytic hydrogen evolution, ACS Sustain. Chem. Eng. 7 (2019) 14023–14030.

[30] S. Mohammadnasabomran, C. Márquez-Álvarez, J. Pérez-Pariente, A. Martínez, Short-channel mesoporous SBA-15 silica modified by aluminum grafting as a support for CoRu Fischer–Tropsch synthesis catalysts, Catal. Sci. Technol. 11 (2021) 4245–4258.

[31] K. Yoshizawa, Y. Shiota, T. Yamabe, Reaction pathway for the direct benzene hydroxylation by Iron–oxo species, J. Am. Chem. Soc. 121 (1999) 147–153.

[32] S. Ito, A. Mitarai, K. Hikino, M. Hirama, K. Sasaki, Deactivation reaction in the hydroxylation of benzene with Fenton's reagent, J. Org. Chem. 57 (1992) 6937–6941.

[33] G.P. Anipsitakis, D.D. Dionysiou, Radical generation by the interaction of transition metals with common oxidants, Environ. Sci. Technol. 38 (2004) 3705–3712.

[34] X. Zhu, N. Guijarro, Y. Liu, P. Schouwink, R.A. Wells, F. Le, Formal, S. Sun, C. Gao, K. Sivula, Spinel structural disorder influences solar-water-splitting performance of $ZnFe_2O_4$ nanorod photoanodes, Adv. Mater. (2018), e1801612.

[35] T.K. Sahu, A.K. Shah, G. Gogoi, A.S. Patra, M.S. Ansari, M. Qureshi, Effect of surface overlayer in enhancing the photoelectrochemical water oxidation of in situ grown one-dimensional spinel zinc ferrite nanorods directly onto the substrate, Chem. Commun. 54 (2018) 10483–10486.

[36] Y. Guo, N. Zhang, X. Wang, Q. Qian, S. Zhang, Z. Li, Z. Zou, A facile spray pyrolysis method to prepare Ti-doped $ZnFe_2O_4$ for boosting photoelectrochemical water splitting, J. Mater. Chem. A 5 (2017) 7571–7577.

[37] J. Li, X. Li, Z. Yin, X. Wang, H. Ma, L. Wang, Synergetic effect of facet junction and specific facet activation of $ZnFe_2O_4$ nanoparticles on photocatalytic activity improvement, ACS Appl. Mater. Interfaces 11 (2019) 29004–29013.

[38] L. Yu, G. Li, X. Zhang, X. Ba, G. Shi, Y. Li, P.K. Wong, J.C. Yu, Y. Yu, Enhanced activity and stability of carbon-decorated cuprous oxide mesoporous nanorods for CO_2 reduction in artificial photosynthesis, ACS Catal. 6 (2016) 6444–6454.

[39] G. Zhu, W. Zhu, Y. Lou, J. Ma, W. Yao, R. Zong, Y. Zhu, Encapsulate alpha-MnO_2 nanofiber within graphene layer to tune surface electronic structure for efficient ozone decomposition, Nat. Commun. 12 (2021) 4152.

[40] L.-W. Zhang, H.-B. Fu, Y.-F. Zhu, Efficient TiO_2 photocatalysts from surface hybridization of TiO_2 particles with graphite-like carbon, Adv. Funct. Mater. 18 (2008) 2180–2189.

[41] J.B. Pan, S. Shen, L. Chen, C.T. Au, S.F. Yin, Core–Shell photoanodes for photoelectrochemical water oxidation, Adv. Funct. Mater. 31 (2021), 2104269.

[42] G. Wen, S. Wu, B. Li, C. Dai, D.S. Su, Active sites and mechanisms for direct oxidation of benzene to phenol over carbon catalysts, Angew. Chem. Int. Ed. Engl. 54 (2015) 4105–4109.

[43] H. Zhang, X. Pan, X. Han, X. Liu, X. Wang, W. Shen, X. Bao, Enhancing chemical reactions in a confined hydrophobic environment: an NMR study of benzene hydroxylation in carbon nanotubes, Chem. Sci. 4 (2013) 1075.

[44] J.-H. Yang, G. Sun, Y. Gao, H. Zhao, P. Tang, J. Tan, A.-H. Lu, D. Ma, Direct catalytic oxidation of benzene to phenol over metal-free graphene-based catalyst, Energy Environ. Sci. 6 (2013) 793.

[45] Y. Wang, H. Sun, X. Duan, H.M. Ang, M.O. Tadé, S. Wang, A new magnetic nano zero-valent iron encapsulated in carbon spheres for oxidative degradation of phenol, Appl. Catal. B: Environ. 172–173 (2015) 73–81.

[46] Y. Yao, H. Chen, C. Lian, F. Wei, D. Zhang, G. Wu, B. Chen, S. Wang, Fe, Co, Ni nanocrystals encapsulated in nitrogen-doped carbon nanotubes as Fenton-like catalysts for organic pollutant removal, J. Hazard Mater. 314 (2016) 129–139.

[47] J.B. Pan, B.H. Wang, J.B. Wang, H.Z. Ding, W. Zhou, X. Liu, J.R. Zhang, S. Shen, J. K. Guo, L. Chen, C.T. Au, L.L. Jiang, S.F. Yin, Activity and stability boosting of an oxygen-vacancy-rich $BiVO_4$ photoanode by NiFe-MOFs thin layer for water oxidation, Angew. Chem. Int. Ed. Engl. 60 (2021) 1433–1440.

[48] Y. Wang, J. Zhang, X. Wang, M. Antonietti, H. Li, Boron- and fluorine-containing mesoporous carbon nitride polymers: metal-free catalysts for cyclohexane oxidation, Angew. Chem. Int. Ed. Engl. 49 (2010) 3356–3359.

[49] H. Yu, F. Peng, J. Tan, X. Hu, H. Wang, J. Yang, W. Zheng, Selective catalysis of the aerobic oxidation of cyclohexane in the liquid phase by carbon nanotubes, Angew. Chem. Int. Ed. Engl. 50 (2011) 3978–3982.

[50] Y. Fu, X. Wang, Magnetically separable $ZnFe_2O_4$–graphene catalyst and its high photocatalytic performance under visible light irradiation, Ind. Eng. Chem. Res. 50 (2011) 7210–7218.
[51] W. Zhang, M. Wang, W. Zhao, B. Wang, Magnetic composite photocatalyst $ZnFe_2O_4/BiVO_4$: synthesis, characterization, and visible-light photocatalytic activity, Dalton Trans. 42 (2013) 15464–15474.
[52] M. Zhu, C. Zhai, L. Qiu, C. Lu, A.S. Paton, Y. Du, M.C. Goh, New method to synthesize S-doped TiO_2 with stable and highly efficient photocatalytic performance under indoor ssunlight irradiation, ACS Sustain. Chem. Eng. 3 (2015) 3123–3129.
[53] W. Zhan, Q. He, X. Liu, Y. Guo, Y. Wang, L. Wang, Y. Guo, A.Y. Borisevich, J. Zhang, G. Lu, S. Dai, A sacrificial coating strategy toward enhancement of metal-support interaction for ultrastable Au nanocatalysts, J. Am. Chem. Soc. 138 (2016) 16130–16139.
[54] J.L. Achtyl, I.V. Vlassiouk, P.F. Fulvio, S.M. Mahurin, S. Dai, F.M. Geiger, Free energy relationships in the electrical double layer over single-layer graphene, J. Am. Chem. Soc. 135 (2013) 979–981.
[55] Y.F. Ping An, Danlei Wei, Yanglong Guo, Wangcheng Zhan, Jinshui Zhang, Hollow nitrogen-rich carbon nanoworms with high activity for metal- free selective aerobic oxidation of benzyl alcohol, Acta Phys.-Chim. Sin. 37 (10) (2021), 2001025.
[56] Y. Yao, Y. Cai, F. Lu, J. Qin, F. Wei, C. Xu, S. Wang, Magnetic $ZnFe_2O_4$–C_3N_4 hybrid for photocatalytic degradation of aqueous organic pollutants by visible light, Ind. Eng. Chem. Res. 53 (2014) 17294–17302.
[57] B. Palanivel, S. devi Mudisoodum perumal, T. Maiyalagan, V. Jayarman, C. Ayyappan, M. Alagiri, Rational design of $ZnFe_2O_4$–C_3N_4 nanocomposite for enhanced photo-Fenton reaction and supercapacitor performance, Appl. Surf. Sci. 498 (2019), 143807.
[58] L. Lv, L. Zhang, X. He, H. Yuan, S. Ouyang, T. Zhang, Energy-efficient hydrogen production via electrochemical methanol oxidation using a bifunctional nickel nanoparticle-embedded carbon prism-like microrod electrode, Acta Phys. Chim. Sin. 37 (7) (2021), 2007079-2007070.
[59] S. Zhang, X.-T. Gao, P.-F. Hou, T.-R. Zhang, P. Kang, Nitrogen-doped Zn–Ni oxide for electrochemical reduction of carbon dioxide in sea water, Rare Met. 40 (2021) 3117–3124.
[60] X. Zhou, X. Li, H. Sun, P. Sun, X. Liang, F. Liu, X. Hu, G. Lu, Nanosheet-assembled $ZnFe_2O_4$ hollow microspheres for high-sensitive acetone sensor, ACS Appl. Mater. Interfaces 7 (2015) 15414–15421.
[61] B. Xu, L. Yu, X. Zhao, H. Wang, C. Wang, L.Y. Zhang, G. Wu, Simple and effective synthesis of zinc ferrite nanoparticle immobilized by reduced graphene oxide as anode for lithium-ion batteries, J. Colloid Interface Sci. 584 (2021) 827–837.
[62] J. Zhao, Q. Yang, R. Shi, G.I.N. Waterhouse, X. Zhang, L.-Z. Wu, C.-H. Tung, T. Zhang, FeO–CeO_2 nanocomposites: an efficient and highly selective catalyst system for photothermal CO_2 reduction to CO, NPG Asia Mater. 12 (2020).
[63] Q. Zhang, J.-B. Liu, L. Chen, C.-X. Xiao, P. Chen, S. Shen, J.-K. Guo, C.-T. Au, S.-F. Yin, An etching and re-growth method for the synthesis of bismuth ferrite/MIL-53(Fe) nanocomposite as efficient photocatalyst for selective oxidation of aromatic alcohols, Appl. Catal. B: Environ. 264 (2020), 118529.
[64] D. Wei, L. Huang, H. Liang, J. Zou, W. Chen, C. Yang, Y. Hou, D. Zheng, J. Zhang, Photocatalytic hydroxylation of benzene to phenol over organosilane-functionalized $FeVO_4$ nanorods, Catal. Sci. Technol. 11 (2021) 5931–5937.
[65] J. Zhang, M. Zhang, C. Yang, X. Wang, Nanospherical carbon nitride frameworks with sharp edges accelerating charge collection and separation at a soft photocatalytic interface, Adv. Mater. 26 (2014) 4121–4126.
[66] Q. Zhu, B. Qiu, M. Du, M. Xing, J. Zhang, Nickel boride cocatalyst boosting efficient photocatalytic hydrogen evolution reaction, Ind. Eng. Chem. Res. 57 (2018) 8125–8130.
[67] I.C. Gerber, P. Serp, A theory/experience description of support effects in carbon-supported catalysts, Chem. Rev. 120 (2020) 1250–1349.
[68] X. Pan, X. Bao, The effects of confinement inside carbon nanotubes on catalysis, Acc. Chem. Res. 44 (8) (2011) 553–562.